Materials Today Bio 29 (2024) 101313

Contents lists available at ScienceDirect

Materials Today Bio

journal homepage: www.journals.elsevier.com/materials-today-bio

Catechol-rich gelatin microspheres as restorative medical implants intended for inhibiting seroma formation and promoting wound healing

Xinping Wang [a,1], Guoqing Wang [b,1], Jianfei Wang [a], Junqiang Xue [c], Gaoli Liu [b], Changjiang Fan [a,*]

[a] Institute for Translational Medicine, The Affiliated Hospital of Qingdao University, Qingdao Medical College, Qingdao University, Qingdao, 266021, Shandong, PR China
[b] Department of Cardiovascular Surgery, The Affiliated Hospital of Qingdao University, Qingdao Medical College, College of Medicine, Qingdao University, Qingdao, 266021, Shandong, PR China
[c] Department of Rehabilitation Medicine, The Affiliated Hospital of Qingdao University, Qingdao Medical College, Qingdao University, Qingdao, 266000, Shandong, PR China

ARTICLE INFO

Keywords:
Wound healing
Microsphere
Seroma
Catechol
Tissue engineering
Gelatin

ABSTRACT

Seroma formation and poor wound healing are common complications of many surgeries that create anatomical dead space (i.e., mastectomy), often causing tissue infection and even necrosis. Although negative pressure drainage and tissue adhesives are investigated to alleviate fluid accumulation post-surgery, however, their therapeutic efficacy remains unsatisfactory in most cases. Herein, the catechol-rich chemically crosslinked gelatin microspheres (ca-CGMSs) have been developed as biodegradable reconstructive implants for preventing seroma formation and concurrently promoting subcutaneous wound healing. Compared with the most representative hydrogel adhesive, i.e. commercial porcine fibrin sealant (PFS), the loosely packed ca-CGMSs with diameters range from 50 to 350 μm, provide numerous cell-adhesive interfaces and interconnected macro-pores for enhanced cell adhesion, proliferation and migration. Subcutaneous embedding trials show the *in situ* swelling aggregation and wet tissue adhesion of ca-CGMSs as well as their capacity in recruiting autologous cells in rat mastectomy models. The trials in rabbit mastectomy models demonstrate that, compared with PFS gluing, the implanted dried ca-CGMSs not only significantly inhibit seroma formation, but also achieve enhanced wound healing by inducing the formation of vascularized neo-tissue. The ca-CGMSs show a great potential to be the next-generation of restorative materials for both preventing seroma formation and healing subcutaneous wounds.

1. Introduction

Excessive fluid accumulated around wounds (i.e., seroma) is one of the most common complications after many surgeries that create anatomical dead space, such as mastectomy [1]. Currently, placement of negative pressure drainage is the standard method to reduce post-mastectomy seroma formation in clinical practices [2]. However, the treatment efficacy is often unsatisfactory, such as delayed wound healing and high probability of bacterial infection, especially for older adults and the patients with diabetes [3]. Furthermore, the protracted poor wound healing may induce flap necrosis and even necessitate reoperation [4].

In recent years, driven by the aging population and the rising incidence of breast cancer, the problems of seroma formation and delayed tissue healing post-surgery have garnered increasing attention, yet only a few treatment methods have been proposed to close the dead space [2,5,6]. Among them, one way is to use hydrogel adhesives to glue the free skin flaps onto subcutaneous tissues [7,8]. Typically, availability of fibrin sealant tissue glue has widely been studied for eliminating seroma formation [9,10]. In our previous studies, a mussel-inspired double--crosslinked tissue adhesive has been developed and explored to prevent seroma formation on rat mastectomy models [11,12]. However, the inherent dense gel body (consists of nano-sized polymer networks) of these adhesive hydrogels usually inhibit cell ingrowth, and thus

* Corresponding author. Institute for Translational Medicine The Affiliated Hospital of Qingdao University Qingdao University Qingdao, 266021, PR China.
E-mail address: cjfan@qdu.edu.cn (C. Fan).
[1] Authors contributed equally to this work.

https://doi.org/10.1016/j.mtbio.2024.101313
Received 21 June 2024; Received in revised form 2 October 2024; Accepted 25 October 2024
Available online 29 October 2024

subsequently hinder *in situ* neo-tissue formation and wound healing [13], albeit they may play a role in preventing seroma formation.

Tissue engineering, generally, executed by means of implanting cell-free or cell-laden scaffolds into tissue defects, is well recognized as one of the most promising strategies to promote wound healing and repair damaged tissue [14–16]. Nevertheless, the cell-free and restorative scaffolding materials, aiming at inhibiting seroma formation and concurrently promoting wound healing, have been very rarely reported. Gelatin has excellent biocompatibility, biodegradability, nontoxicity, and low immunogenicity, which can promote cell adhesion and spreading due to the presence of Arg-Gly-Asp (RGD) motifs [17]. Gelatin-based microspheres (GMSs) are often incorporated into traditional three-dimensional (3D) scaffolds (e.g., hydrogel, sponge, nanofibers) as carriers of cells, drugs, or/and growth factors [18]. In previous studies, we has found that the thermally stable GMSs can be "glued" by significantly promote osteoblast proliferation to form a whole construct, and thus which have been used standalone to facilitate the repair of bone defects [19–21]. In recent years, the usage of GMSs as tissue engineering scaffolding materials has received a surge of interest [22–29]. Due to the unique combination of hydroxyl and phenol, catechols possess many charming properties for developing tissue adhesives and hemostatic sealants [12,30,31]. For instance, catechol can penetrate water layers of surfaces and then participate in various interface interactions (e.g., hydrogen bond, metal coordination, π-π interaction, cation-π interaction) to enhance the adhesion of catechol-rich materials onto wet substrates (e.g., biological tissues) [31–33]. Furthermore, catechol groups also exhibit antioxidant, antibacterial, and anti-inflammatory activities, aiding wound healing [34–36].

In this study, we aim to develop the catechol-rich chemically crosslinked gelatin microspheres (ca-CGMSs) and explore their potential as restorative medical implants to inhibit seroma formation and simultaneously promote subcutaneous wound healing. We hypothesize that the dried ca-CGMSs will absorb seroma fluid around wound and then create adhesion to wet tissue, and meanwhile the *in situ* swollen ca-CGMSs will achieve the desired wound healing by promoting the recruitment and proliferation of autologous cells as well as neo-tissue formation (Fig. 1). To test this hypothesis, catechol-rich gelatin (namely gelatin-dopamine, gel-dopa) has been synthesized for fabricating water-absorbable ca-CGMSs, and then the dried ca-CGMSs are surgically implanted into well-established rat and rabbit mastectomy models for evaluating their capability in recruiting endogenous cells, adhering to wet tissue, eliminating seroma fluid accumulation, and aiding subcutaneous wound healing, by employing commercial porcine fibrin sealant (PFS) (that is a representative gel adhesive) and negative pressure drainage system (that is a commonly used method in clinical practice, termed as blank) as controls. Besides, the morphology and biodegradability of ca-CGMSs and their effects on cell viability, adhesion, proliferation, and migration are investigated in detail.

2. Materials and methods

2.1. Synthesis of gel-dopa

The gel-dopa conjugate has been synthesized by using the ethyl-dimethyl-aminopropylcarbodiimide (EDC, Aladdin, China)/N-hydroxy-succinimide (NHS, Aladdin, China) activation chemistry [11]. Briefly, gelatin (2.0 g, Sigma-Aldrich) is dissolved in 250 mL of phosphate buffered saline (PBS) solution at 40 °C, followed by the addition of EDC (1.5 g). After stirring for 30 min in a water bath at 40 °C, NHS (1.0 g) and dopamine hydrochloride (1.5 g, Aladdin, China) is added. The pH value of solution is maintained from 4.0 to 6.0 across the 36 h of reaction. The mixture solution is dialyzed (molecular weight cut-off: 6000–8000 Da) for two days against the deionized (DI) water that has been supplemented with hydrochloric acid for adjusting the pH value between 4 and 5, and then lyophilized. The resultant solid foam is stored at −20 °C.

2.2. Characterization of gel-dopa

Proton nuclear magnetic resonance spectroscopy (^{1}H NMR) studies are performed to verify the grafting of dopamine onto gelatin. Briefly, the lyophilized gel-dopa, gelatin, and dopamine is dissolved in deuterium oxide (D_2O) and transferred into 5 mm NMR tubes, respectively. The spectra are recorded on a Bruker Avance II 400 NMR spectrometer.

The presence of unoxidzied catechols on gel-dopa is examined by ultraviolet–visible (UV–Vis) spectroscopy. Briefly, solutions (10 %, g/mL) of gelatin and gel-dopa in DI water are analysed, respectively, at wavelengths from 200 nm to 600 nm with a micro-spectrophotometer (K5800, Kaiao, China).

Catechol content of gel-dopa is measured by Arnow's method [11]. Typically, 1.0 mL of hydrochloric acid solution (0.5 M) containing

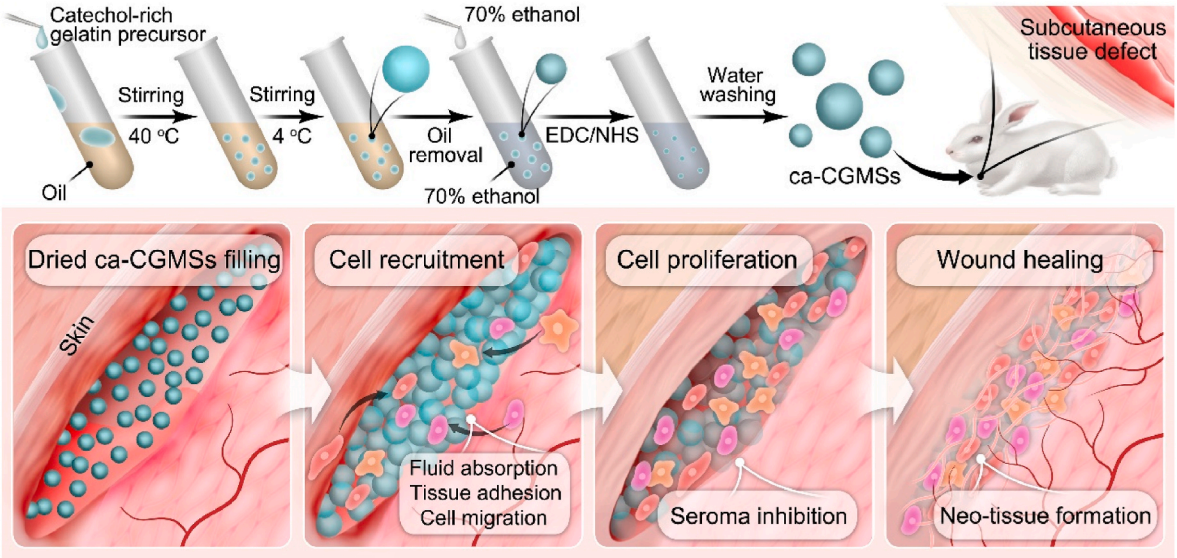

Fig. 1. Schematic development of ca-CGMSs and their applications for both preventing seroma formation and healing subcutaneous wounds. The ca-CGMSs are prepared from the catechol-rich precursor solution with the water-in-oil emulsion method, followed by chemical crosslinking. After being transplanted into subcutaneous tissue defects, the ca-CGMSs not only form an aggregated construct and stick onto the wet tissue after absorbing seroma fluids, but also recruit autologous cells that achieve ingrowth into the tissue defect by migration and proliferation, realizing neo-tissue formation and wound healing.

sodium nitrite (10 %, g/mL, Aladdin, China) and sodium molybdatein (10 %, g/mL, Aladdin, China) is mixed with 1.0 mL of gel-dopa solution (0.2 %, g/mL) in DI water. After shaking for 5 min at 150 rpm, the pH value and volume is tuned to 7.0 and 5 mL, respectively. The absorbance at 520 nm is detected with a micro-spectrophotometer (K5800, Kaiao, China). Dopamine hydrochloride is employed as the control.

2.3. Preparation of ca-CGMSs

The fabrication of ca-CGMSs involves two steps: First, the physically crosslinked catechol-functionalized microspheres (ca-PGMSs) are prepared with the water-in-oil (w/o) emulsion method [19]. Briefly, 1.5 g of gel-dopa and 1.5 g of gelatin is dissolved in 20 mL of DI water at 40 °C, and then poured into a 250 mL of beaker containing 80 mL of mixed oil (paraffin oil: edible oil = 3:1), followed by continuous stirring for 30 min at 700 rpm, 40 °C on a magnetic stirrer. Next, the beaker containing the mixture solution is transferred into an ice/water bath on a magnetic stirrer. After 30 min of stirring at 700 rpm, the precipitate is isolated with a steel sieve, washed alternately with 1, 4-dioxane (50 mL) and acetone (50 mL) for three times, washed twice with anhydrous ethanol (50 mL), and dried in vacuum at room temperature. Second, the resultant ca-PGMSs are chemically crosslinked with EDC/NHS. Briefly, ca-PGMSs (0.5 g) are suspended within 70 % (v/v) ethanol prepared with PBS (30 mL, pH = 5–6) at room temperature, followed by adding the predetermined amounts of EDC and NHS and then shaking at 150 rpm for a scheduled period of time. The obtained ca-CGMSs are washed thrice with water, freeze-dried, sifted with two standard sieves (100–200 meshes, 150-75 μm), and stored at 4 °C until use. The overall preparation yield of ca-CGMSs is about 46 %.

2.4. Characterization of ca-CGMSs

The morphology of ca-CGMSs is observed by scanning electron microscopy (SEM) after sputtered coating of gold onto the dried ca-CGMSs.

The dried ca-CGMSs (W_d) is soaked in PBS at 37 °C for three days to reach swelling equilibrium, The morphologies of swollen ca-CGMSs are recorded with a microscope (Nikon Eclipse Ti2). In addition, the supernatant is carefully pipetted out, and then weighed (W_s). The swelling ratio is determined as follows:

$$\textit{Swelling ratio}\ (\%) = W_s/W_d \times 100\%$$

The equilibrium swollen ca-CGMSs (W_{es}) is immersed in trypsin solution (0.001 %) at 37 °C. At predetermined time points, the supernatant is carefully removed and the residual ca-CGMSs is weighed (W_{rt}). The remaining weight (RW) is calculated as follows:

$$\text{RW}\ (\%) = W_{rt}/W_{es} \times 100\%$$

The particle size (diameter) of ca-CGMSs is determined on the optical microscope images, in which at least two hundred of ca-CGMSs are randomly selected and measured with ImageJ.

2.5. Cell culture

Mouse fibroblasts (L929 cells) are seeded into a 10-cm tissue culture dish containing the cell culture medium (RPMI 1640 medium (Gibco) supplemented with 10 % (v/v) fetal bovine serum (FBS, Meilunbio, Dalian, China), 1 % (v/v) penicillin-streptomycin (Invitrogen)), and then placed in a 37 °C, CO_2 (5 %) cell-culture incubator.

2.6. Fabrication and culture of cell-laden constructs

The 24-well plate is coated by adding 200 μL of agarose solution (1 %) into each well. 1.0 g of sterile ca-CGMSs is suspended into 1.0 mL of cell culture medium. 60 μL of ca-CGMSs suspension is transferred into per well of a 24-well plate. As the control group, 100 μL of PFS is prepared in each well of a 24-well plate according to the instructions. Subsequently, 2.5×10^5 cells suspended in 1.0 mL of medium are added into each well of the 24-well plate. They are placed into the cell-culture incubator.

2.7. Cell viability

Cell viability is estimated with a live/dead cell double staining assay. Briefly, the cells laden ca-CGMSs and PFS are transferred into a 24-well plate, followed by the addition of 1.0 mL of RPMI 1640 medium containing 2 μM calcein-AM and 4 μM propidium iodide, respectively. After incubating at 37 °C for 30 min and washing twice with RPMI 1640 medium, the cells are observed with a fluorescence microscope (Nikon Eclipse Ti2).

2.8. Cell proliferation

The proliferation of L929 cells on ca-CGMSs and PFS is determined with PrestoBlue assay (Life Technologies) by following the instructions. Briefly, cell culture medium in each well of the 24-well plate is replaced with 1.0 mL of PrestoBlue working solution at each pre-determined time point, which is placed back into the CO_2 incubator for 30 min. The fluorescence intensity of supernatant is recorded at 590 nm with excitation at 560 nm. The relative cell viability is calculated according to manufacturers' instructions, and which is defined as 1.0 for the PFS group at day one.

2.9. F-actin staining

The cytoskeleton filament F-actin of L929 cells is stained with rhodamine-phalloidin (40734ES75, Yeasen, China) according to manufacturer's instructions. Briefly, the cell-laden constructs or tissue slices that have been fixed with 4 % paraformaldehyde, are washed with PBS thrice, and treated with the PBS containing 0.5 % (w/v) Triton X-100 (Sigma-Aldrich) and 3 % (w/v) BSA (Solarbio, China) for 30 min. The samples are incubated with the working solution of rhodamine-phalloidin in the dark for 30 min, followed by nuclear staining with 4′, 6-diamidino-2-phenylindole (DAPI, Sigma-Aldrich) solution (1 μg/mL). Cellular morphology and distribution are estimated by observing with a fluorescence microscope (Nikon Eclipse Ti2).

2.10. Cell migration

The migration of L929 cells across ca-CGMSs is measured with transwell assay. Briefly, sterile ca-CGMSs and PFS are placed in upper chambers (pore size: 8 μm), respectively, and putted into a 24-well plate. 200 μL of L929 cell suspension (5×10^4 cells) in RPMI 1640 medium is added into the upper chamber. Subsequently, 600 μL of cell culture medium is added into each well. The 24-well plate is incubated at 37 °C in 5 % CO_2 for 24 h. After removing ca-CGMSs or PFS within the upper chambers, the cells on the inner side of upper chambers are gently wiped off with a cotton swab. The cells on the outer side of the upper chambers are stained with 0.1 % crystal violet, and then observed under an optical microscope (Nikon Eclipse Ti2).

2.11. Animal studies

All animal studies are carried out according to the guidelines approved by the Medical Ethics Committee of Affiliated Hospital of Qingdao University (No. QYFY WZLL 28842). These experiments are compliant with all relevant ethical regulations regarding animal research. Female Sprague-Dawley rats (8–10 weeks old) are ordered from SPF (Beijing) Biotechnology Co., Ltd.; female New Zealand White rabbits (6–8 months old) are purchased from Qingdao Kangda Biotechnology Co., Ltd. (Shandong, China).

2.12. Tissue adhesion and cell capture of ca-CGMSs in rat mastectomy models

Rat mastectomy models are established according to previous studies [12,37]. The rats (weighing approximately 250 g, n = 12) are anesthetized by intraperitoneally injecting pentobarbital sodium (40 mg/kg). They are placed in the supine position, depilated, and the operative area is disinfected with povidone-iodine and 75 % ethanol. A midline incision is made from jugular notch to the xiphoid process using a scalpel and surgical scissors. Subsequently, the right chest flap is lifted and separated from the musculature with hemostatic forceps to expose the edges of the pectoralis muscle, axilla, clavicle, and latissimus dorsi muscle. The pectoralis major, pectoralis minor, adipose tissue, mammary gland, and visible lymph nodes are excised carefully, resulting in a defect size of 2.0 cm × 1.2 cm. The defect is filled with ca-CGMSs, and followed by wound closure with interrupted sutures. Animals are monitored daily for signs of wound dehiscence and infection. The photographs of embedded ca-CGMSs are recorded with a digital camera. In addition, the ca-CGMSs are harvested, washed with RPMI 1640 medium, and stained with calcein-AM and rhodamine-phalloidin, respectively.

2.13. Seroma prevention and wound healing in rabbit mastectomy models

The New Zealand rabbits (approximately 2 kg) are randomly assigned to three groups: blank (n = 6), PFS (n = 6), and ca-CGMSs (n = 6). Anesthesia is performed *via* intraperitoneal injection of sodium pentobarbital (40 mg/kg). The procedures are similar to that of the establishment of rat mastectomy models described above. The tissue defect size of 5 cm × 3 cm is established subcutaneously in a rabbit mastectomy model. Subsequently, the defects are glued with PFS or filled with ca-CGMSs, which are designated as the PFS group and ca-CGMS group, respectively. The blank control group is not subjected to any treatment. Each animal model receives a drainage tube, which is inserted subcutaneously and connected externally to a negative pressure ball for fluid collection for five days. The wounds are closed with interrupted sutures. Animals are monitored on a daily basis for wound dehiscence and infection, and the fluid in the drainage tube and negative pressure ball is weighted. At 7 and 28 days post-surgery, the rabbits are euthanized, and the defects along with surrounding tissues are collected for subsequent histological analysis.

2.14. Histological and immunochemical analysis

The harvested specimens are washed in PBS, fixed by immersion into a 4 % (w/v) paraformaldehyde solution at 4 °C for 48 h. Subsequently, they are dehydrated, paraffin-embedded, sliced into 5-μm thick sections using a paraffin microtome, and then affixed to the anti-detachment glass slides. Afterward, the sections are rehydrated in PBS solution and subjected to hematoxylin-eosin (H&E) staining (G1003, Servicebio, China), Masson's trichrome staining (G1006, Servicebio), sirius red staining (G1018, Servicebio), and F-actin staining (40734ES75, Yeasen, China), respectively, according to manufacturer's instructions.

For immunohistochemistry (IHC) staining, the rehydrated sections are incubated for 60 min in the PBS solution containing 3 % (w/v) bovine serum albumin (BSA, Solarbio, China) and 0.1 % (w/v) Triton X-100 (Sigma-Aldrich) to prevent nonspecific adsorption. Subsequently, the sections are washed twice with PBS (15 min each), followed by incubation with a primary antibody for 1 h at 37 °C against CD31 (AF6191, Affinity, China), VEGF (AF5131, Affinity, China), and Hif-1α (AF1009, Affinity, China), respectively. This is followed by PBS washing for two times and incubation with the secondary antibody (rabbit anti-goat IgGHRP, 5 μg/mL in PBS, GB23204, Servicebio) at 37 °C for 1 h, respectively. After washing twice with PBS, the samples are sequentially treated with 3, 3′-diaminobenzidine (DAB) (G1211, Servicebio) solution for 5 min and hematoxylin (G1003, Servicebio) for 30 s, and followed by rinsing with tap water for 2 min. For immunofluorescence staining, the rehydrated sections are incubated in the solution of 3 % (w/v) BSA and 0.1 % (w/v) Triton X-100 for 1 h, followed by incubating with the primary antibody against collagen type I (Col1, A24112, ABclonal, China) and von Willebrand Factor (vWF, sc-365712, Santa Cruz) for 1 h at 37 °C, washed thrice with PBS, and incubated with 5 μg/mL of Goat Anti-rabbit IgG (BA1127, BOSTER) and anti-mouse lgG in PBS (BA1126, BOSTER) for 1 h, respectively, followed by DAPI staining for 30 s and PBS washing thrice in darkness. The samples are observed by optical microscopy (Nikon Eclipse Ti2), and besides, the samples undergoing sirius red staining are also observed with a polarization microscope (Leica DM2700 P). ImageJ software is used to analyze the intensities of histological or immunochemical signals for quantifying cell density or deposition of target proteins.

2.15. Statistical analysis

At least three independent repetitions of each group are performed, and quantitative data are presented as the mean ± standard deviation (SD). Statistical significance between two groups are determined using the Student's t-test. A p-value <0.05 between two groups is considered statistically significant.

3. Results and discussion

3.1. Preparation and characterization of ca-CGMSs

Aiming to develop gelatin-based microspheres with the capabilities of absorbing seroma fluid, facilitating adhesion onto wet tissues, and aiding wound healing, we have designed and fabricated the ca-CGMSs *via* three steps. First, the gel-dopa precursor rich in catechol moieties is synthesized by EDC/NHS-mediated coupling reaction between the carboxyl groups on gelatin and amino groups on dopamine (Fig. 2A). To avoid the oxidation of the gel-dopa precursors, the reaction products are dialyzed in acidic DI water (pH = 4–5). Second, the temperature-sensitive ca-PGMSs are prepared using the w/o emulsion method; and last, the thermally stable ca-CGMSs are achieved by covalently crosslinking the ca-PGMSs (Fig. 1A).

We verify the successful synthesis of gel-dopa precursor *via* qualitative and quantitative examinations. As displayed in Fig. 2B, the peak at δ 2.8 ppm (marked with an arrow) that can be assigned to protons of the methylene (labeled with an asterisk) close to phenyl group in dopamine [11], has been clearly observed in the spectrum of reaction product rather than gelatin, demonstrating successful grafting of dopamine onto gelatin. Furthermore, UV–Vis spectroscopy is carried out to check the oxidation states of catechols on gel-dopa conjugates. As expected, UV–Vis absorption of the gel-dopa at 280 nm wavelength is higher than that of gelatin (Fig. 2C), again proving the presence of abundant catechol groups on the gel-dopa precursor [30]. Meanwhile, significantly, no signal is detected at the wavelengths greater than 320 nm, indicating the minimal oxidization of catechol groups on the gel-dopa [38]. In addition, content of the catechol on gel-dopa (4.1 μg/mg) is quantitatively measured by using Arnow's method, and as anticipated, which is dramatically higher than that on gelatin (0.9 μg/mg). Considering the decrease in carboxyl content due to dopamine conjugation, the mixed solution of gel-dopa (7.5 %, w/v) and gelatin (7.5 %, w/v), which can undergo sol-gel transition when temperature decreases to ambient temperature (20–25 °C) from 40 °C (Fig. S1, Supplementary material), is employed to fabricate the temperature-sensitive ca-PGMSs. The solubility of ca-PGMSs in aqueous solution at 37 °C has limited their wide applications as scaffolding materials, and therefore, they are designed to be covalently crosslinked by using EDC/NHS chemistry to obtain the thermally stable ca-CGMSs (Fig. 2D, Fig. S2; Supplementary material). As observed by SEM, the ca-CGMSs show round or oval morphology with a smooth surface (Fig. 2E), albeit the wrinkles can be detected by careful observation. This smooth surface should also be attributed to the fact that the as-prepared ca-CGMSs observed by SEM do not swell in water.

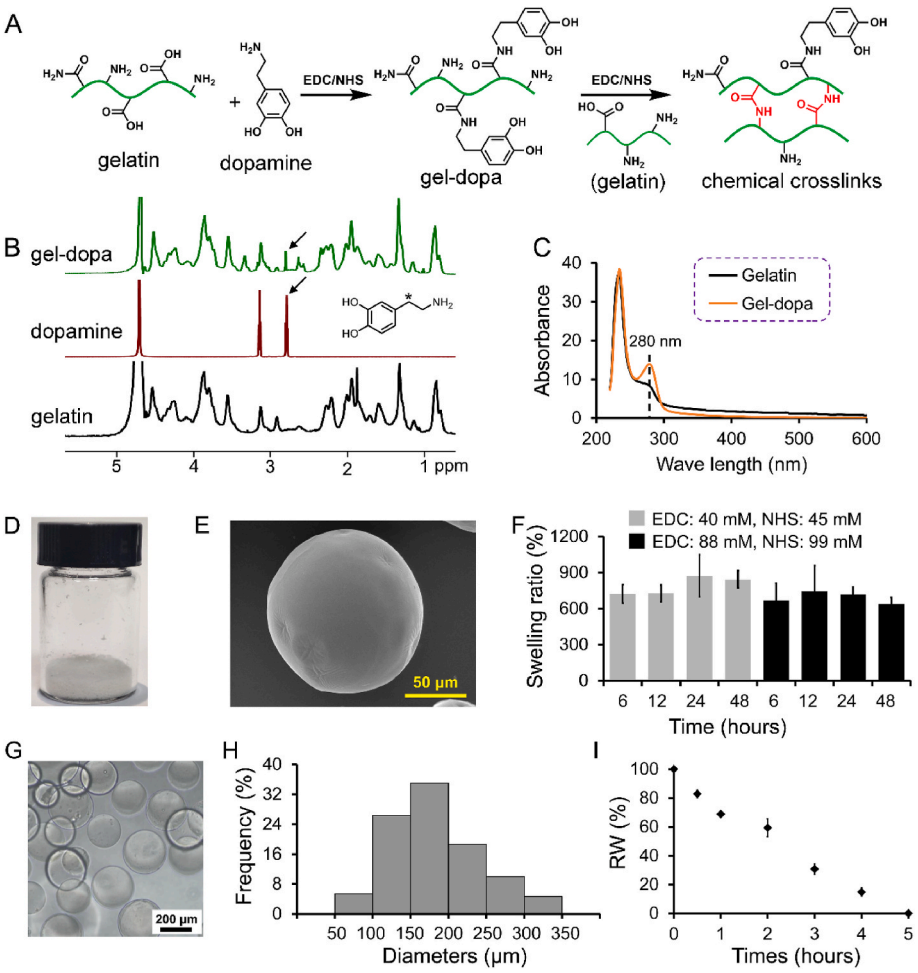

Fig. 2. Preparation and characterization of ca-CGMSs. (A) Synthetic route of gel-dopa precursor and chemical crosslinking in formation of ca-CGMSs. (B) ^{1}H NMR spectra of gelatin, dopamine, and gel-dopa. (C) UV–Vis spectra of the solution (10 %, w/v) of gelatin and gel-dopa precursor, respectively. (D) Dried powder of ca-CGMSs. (E) SEM image of ca-CGMSs. (F) Equilibrium swelling ratios of ca-CGMSs fabricated with varied EDC/NHS concentrations and crosslinking times. (G) Optical image of the ca-CGMSs in PBS. (H) Diameter distribution of swollen ca-CGMSs in PBS. (I) Degradation profile of ca-CGMSs in trypsin solution at 37 °C.

Besides, in the dry state, their particle size is mainly distributed in the range of 50–150 μm (Fig. S3, Supplementary material).

The feasibility and needed time for successful crosslinking of ca-PGMSs in the ethanol/PBS (7:3) solution at room temperature (20–25 °C), has been evaluated. Interestingly, the swelling ratio of ca-CGMSs is not significantly affected by the dosage of crosslinking agents (EDC/NHS) from 40 mM/45 mM–88 mM/99 mM and crosslinking times from 6 to 48 h (Fig. 2F). Considering the feasibility and availability, the ca-CGMSs obtained through 6 h of crosslinking with EDC (40 mM) and NHS (45 mM) are used hereafter. The ca-CGMSs absorb PBS up to about 7-fold of its own weight by self-swelling (Fig. 2F, Fig. S4, Supplementary material). Their regular morphology is maintained after swelling in PBS as observed by optical microscopy (Fig. 2G). The particle sizes of equilibrium swollen ca-CGMSs in PBS are varied from 50 to 350 μm, predominantly falling within the range of 100–250 μm (Fig. 2H). Subsequently, we investigated the biodegradability of ca-CGMSs in 0.001 % (w/v) of trypsin solution at 37 °C, 150 rpm of shaking. The degradation ratio exhibits an almost linear correlation with degradation time. The complete degradation of ca-CGMSs is achieved after approximately 5 h of incubation (Fig. 2I). The excellent biodegradability and self-swelling in PBS lays a solid foundation for the potential utilization of ca-CGMSs as scaffolding materials in aiding tissue regeneration.

3.2. Cytocompatibility of ca-CGMSs

To assess the cytocompatibility of ca-CGMSs, we first investigate the viability of the L929 fibroblasts cultured within ca-CGMSs by live/dead cell staining assay, with PFS serving as a control. In this assay, live cells emit green fluorescence, whereas dead cells exhibit red fluorescence (Fig. 3A). One day post-cell seeding, staining reveals that L929 cells has adhered to ca-CGMSs, presenting a typical multilateral morphology with minimal occurrences of cell death. In the PFS group, while most cells has adhered and elongated, exhibiting normal morphology, the incidence of cell death is significantly higher than that in the ca-CGMS group. These results suggest that ca-CGMSs fosters a favorable microenvironment for the survival, adhesion, and spreading of the laden L929 fibroblasts. By 3 day of culture, a significant increase in live cell density is evident on ca-CGMS relative to Day 1, accompanied by a reduced number of dead cells. While an increase in live cell density is observed on PFS, the incidence of dead cells remains higher than that in the ca-CGMS group. Similarly, by Day 5, cell density has increased on both ca-CGMS and PFS groups compared to that on Day 3, respectively, yet the number of dead cells in the PFS group keeps significantly higher than that in the ca-CGMS group. In addition, it is noteworthy that ca-CGMSs can be "glued" together by cells, forming a macroscopic whole structure. These results indicate that ca-CGMSs not only provides a more favorable microenvironment for the survival of L929 fibroblasts by promoting cell adhesion and spreading, but also that their unique 3D structures and

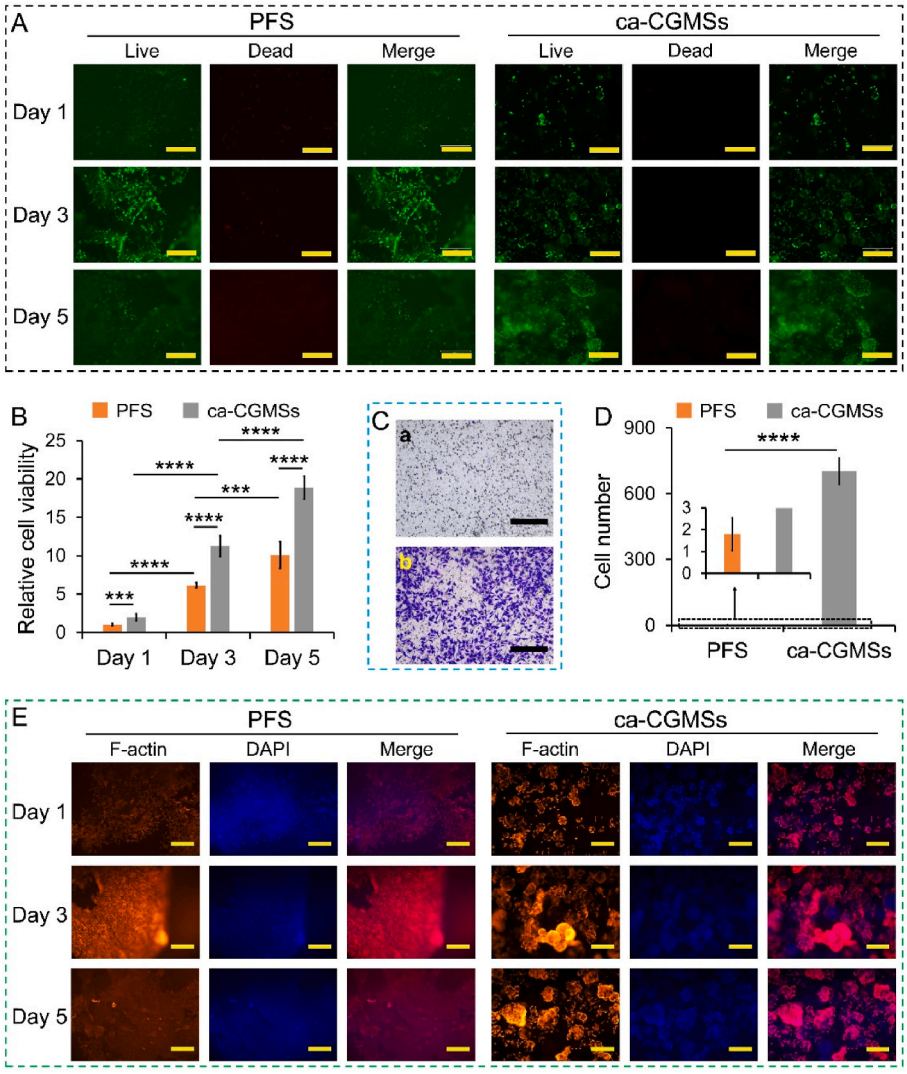

Fig. 3. The microenvironments of ca-CGMSs favor cell survival, proliferation, and migration. (A) Live/dead analysis of L929 cells over culture time; living cells and dead cells are stained green and red, respectively; scale bar is 300 μm (B) Proliferation estimations of L929 cells on PFS and ca-CGMSs, respectively; statistical significance is indicated with *** ($p \leq 0.001$) and **** ($p \leq 0.0001$) ($n = 5$). (C) Crystal violet staining of the cells passing through (a) PFS or (b) ca-CGMSs into the lower transwell chamber; scale bar is 300 μm. (D) Quantification of the cells at the lower transwell chamber; statistical significance is indicated with **** ($p \leq 0.0001$) ($n = 5$). (E) F-actin staining of L929 cells on PFS and ca-CGMSs, respectively, over culture time; scale bar is 300 μm.

larger specific surface area afford greater living interfaces and spaces for cell growth compared with PFS, thereby promoting cell proliferation. Furthermore, the formation of a centimetre-sized whole construct *via* integrating hundreds of micron-sized ca-CGMSs with cells, lays the foundation for *in situ* formation of neo-tissues.

3.3. ca-CGMSs scaffold promotes cell proliferation and migration

Next, we quantitatively analyze cell proliferation using the PrestoBlue assay, in which the quantitative fluorescence intensity in the PFS group at Day 1 is employed as the reference and set as 1.0 to determine the relative cell numbers at various time points for each group (Fig. 3B). The cell count in ca-CGMSs scaffold is roughly 2-fold higher than that in PFS group at Day 1. In both the ca-CGMS and PFS groups, the cell count exhibits an increasing trend from day 1 to days 3 and 5, consistent with the observation of increased cell density in the live/dead cell staining assay. Furthermore, the increasing degree of cell proliferation from Day 1–3 (PFS group: 6-fold; ca-CGMS group: 5.7-fold) for both materials is significantly higher than that from Day 3–5 (PFS group: 1.6-fold; ca-CGMS group: 1.7-fold), respectively. In addition, the significantly higher cell counts in the ca-CGMS group are observed than the PFS group at Day 3 and Day 5. These findings further corroborate that ca-CGMSs scaffold can provide a favorable microenvironment for proliferation of L929 fibroblasts.

To investigate the inducing effect of ca-CGMSs scaffold on cell ingrowth, subsequently, we examine the migratory capacity of L929 cells across ca-CGMSs and PFS scaffold, respectively, using transwell assays (Fig. S5, Supplementary material) [39,40]. As can be seen in Fig. 3C, after 24 h of culture, a substantial quantity of cells migrate and infiltrate through the ca-CGMSs scaffold into the lower chamber in ca-CGMS group. However, almost no cells migrate into the lower chamber in the PFS group (Fig. 3D). These results demonstrate that, compared with the PFS with gel structure, the ca-CGMSs scaffold with loosely packed microsphere structure not only promote cell adhesion, spreading, and proliferation, but also exhibit a superior capability in facilitating cell migration.

3.4. ca-CGMSs provide numerous cell living interfaces and spaces

The morphology of L929 cells on both ca-CGMSs scaffold and PFS is

investigated through F-actin staining (Fig. 3E) to assess their cell affinitive interfaces and living spaces. The L929 cells express cytoskeletal microfilament F-actin on both ca-CGMSs and PFS after 1 day of culture, facilitating their adhesion and spreading. At that time, the cells in both groups display flattened and multilateral shapes, and meanwhile, a lot of growth spaces exist between cells. However, the cells in the PFS group become progressively crowded at Day 3, a phenomenon that is not conducive to further cell proliferation. Conversely, while cell density also rise in the ca-CGMS group, there remain ample spaces for cell growth, indicating the ca-CGMSs scaffold's capacity to provide greater cell living interfaces and rooms for cell adhesion and proliferation. Careful observation reveals that, following a 3 days of incubation, some ca-CGMSs has been "glued" together by cells. Furthermore, after 5 days of incubation, the cells within ca-CGMSs scaffold retain their normal polygonal shapes. However, the cells in the PFS group have started to change into a round shape, suggesting a potential progression towards apoptosis [41]. Thus, compared to PFS, the ca-CGMSs scaffold can provide a superior 3D microenvironment that is rich in cell adhesive interfaces and living spaces to achieve sustained cell survival and proliferation.

3.5. *In vivo tissue adhesion and rapid cell recruitment of ca-CGMSs*

To preliminary estimate the availability of ca-CGMSs in inhibiting seroma formation and healing wound *in vivo*, the capability of ca-CGMSs in adhering to wet tissue and recruiting endogenous cells are first investigated by embedding ca-CGMSs into the well-established rat mastectomy models (Fig. 4A). After two days of transplantation, the ca-CGMSs have formed an aggregated 3D macro constructs after absorbing subcutaneous fluid, and significantly, which firmly attach to the surface of wet tissue with the ability of holding the isolated tissue (Fig. 4B). Interestingly, the intense rinse in the medium cannot cause the ca-CGMSs construct to fall off (Video S1, Supplementary material), indicating their robust adhesion capacity onto wet tissues. Next, the ca-CGMSs-based constructs are separated from tissue surface by scraping (Fig. 4C, Fig. S6, Supplementary material) and undergoes cell staining with calcein-AM and rhodamine-phalloidin, respectively, for evaluating the capture of endogenous cells (Fig. 4D and E). Significantly, a great number of cells are detected with attachment onto the surfaces of ca-CGMSs in the construct. These findings demonstrate the high capacity of ca-CGMSs in achieving firm adhesion onto wet tissues after *in vivo* swelling by absorbing fluid, and at the same time providing a suitable microenvironment (e.g., cell adhesive interfaces, interconnected macropores) for the rapid recruitment of the autologous cells. These superior capabilities of the ca-CGMSs will not only fill the subcutaneous dead space but also facilitate *in situ* formation of subcutaneous neo-tissue and wound healing [21].

Supplementary data related to this article can be found online at https://doi.org/10.1016/j.mtbio.2024.101313

3.6. *Efficacy of ca-CGMSs in seroma prevention in rabbit mastectomy models*

To investigate the role of ca-CGMSs in preventing seroma formation, the rabbit mastectomy models with large subcutaneous tissue defects (5 cm × 3 cm) are established, and the defects are surgically filled with dried ca-CGMSs, glued with PFS, or not treated (blank control group), respectively. To mimic clinical scenarios, the negative pressure drainage is placed to wound site for five days to facilitate the discharge of subcutaneous fluid (Fig. 4F). As shown in Fig. 4G, the volume of collected seroma shows a decreasing tendency over time in all groups.

On postoperative days 1, 2, and 3, a significantly higher volume of

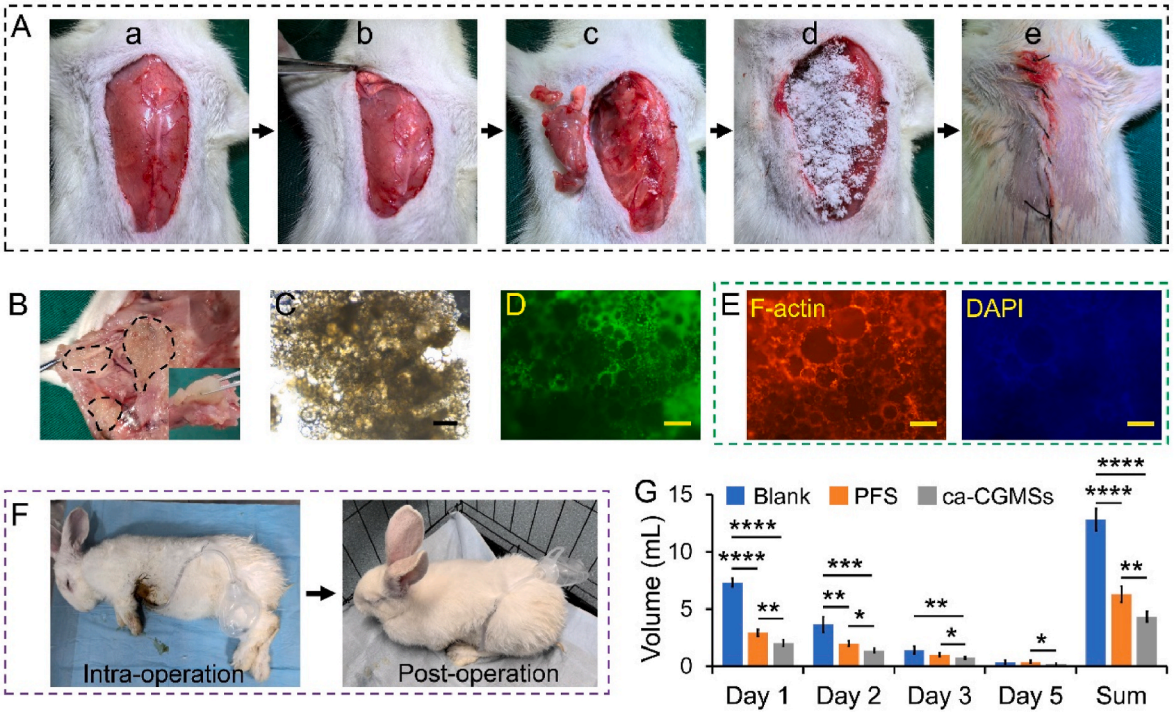

Fig. 4. The dried ca-CGMSs inhibit seroma formation by absorbing fluid and adhering onto wet tissues, and meanwhile rapidly recruit endogenous cells. (A) The sequence of establishment of rat mastectomy model: (a) rats are placed in a supine position; (b) make a midline incision from jugular notch to xiphoid process; (c) remove muscles, fat, the upper mammary glands, and visible lymph nodes; (d) place the dried ca-CGMSs powder; (e) suture surgical areas. (B) Images of the ca-CGMSs after two days of transplantation; the aggregated ca-CGMSs constructs are highlighted with dashed circles that can withstand the weight of the isolated tissue. (C) Bright field image of isolated ca-CGMSs constructs; scale bar is 400 μm. (D) Fluorescent micrographs of the recruited cells in ca-CGMSs constructs after calcein-AM staining; scale bar is 300 μm. (E) F-actin staining of the isolated ca-CGMSs constructs; scale bar is 300 μm. (F) Photographs of the rabbit in steps of intra-operation and post-operation; the negative pressure drainage system is placed. (G) Volume of the collected seroma at each time point and total seroma volume of the three groups, respectively; statistical significance is indicated with * ($p \leq 0.05$), ** ($p \leq 0.01$), *** ($p \leq 0.001$), and **** ($p \leq 0.0001$) ($n = 5$).

fluid has been collected in the blank control group compared to both the ca-CGMS and PFS groups. Specifically, on Day 1, the quantity of subcutaneous fluid in the blank group is 3.6-fold greater than that in the ca-CGMS group and 2.5-fold greater than that in the PFS group. Notably, at each time point, the mean seroma volume in the ca-CGMSs group consistently remains lower than that in both the blank control and PFS groups. Furthermore, the volume of collected seroma in the ca-CGMSs group is significantly smaller than that in PFS groups at each time point. By Day 5, a substantial decrease in fluid volume has been observed across all groups. Moreover, the total seroma volume accumulated over 5 days is significantly lower in the ca-CGMS group compared to both the blank control and PFS groups. These results have demonstrated that, compared to blank control and PFS gluing, the implanted dried ca-CGMSs exhibit outstanding capability of inhibiting subcutaneous seroma formation by absorbing fluid and adhering to subcutaneous tissues.

3.7. ca-CGMSs mediated ingrowth of autologous cells into tissue defect

The formation of neo-tissue in the subcutaneous dead space is highly desirable due to its ability in inhibiting recurrent seroma formation and promoting wound healing. At Day 7 and 28 post-mastectomy in the rabbit models, we sample from the defect sites and adjacent full-thickness tissues. Cell density and distribution is first identified through phalloidin staining to investigate the ingrowth of autologous cells into the tissue defect sites. It can be noted that F-actin and cells (nuclei) in the tissue defect site are obviously denser stained in the ca-CGMS group than both the blank control and PFS groups across all time points (Fig. 5A and B). At Day 7 post-surgery, the cell density is significantly lower in the blank control group in contrast to the PFS and ca-CGMS groups (Fig. 5B). In detail, the cell abundance is highest in the ca-CGMS group, followed by the PFS group, and finally the blank group, respectively. The similar phenomenon has also been observed in F-actin staining (Fig. S7, Supplementary material). Additionally, only in the ca-CGMS group, the cells are uniform distributed across the whole construct. The F-actin and cells are primarily concentrated at the edges of tissue defect, with lesser distribution within the interior in the blank and PFS groups. These results demonstrate the rich interfaces and interconnected porous structures of ca-CGMSs scaffold greatly promote the migration of autologous cells into the interior of the subcutaneous tissue defects (dead spaces), and on the contrary, the autologous cells are difficult to migrate into the dead spaces in the blank and PFS groups. By Day 28, both the densities of F-actin and cells in ca-CGMSs groups are significantly higher than those at Day 7, respectively, demonstrating cell migration into dead spaces or/and *in situ* proliferation. Compared to ca-CGMS group, however, the cells are still sparsely distributed in the blank and PFS groups. As expected, the density of F-actin remains significantly higher in ca-CGMS group than both blank and PFS groups. Furthermore, in the ca-CGMS group, not only is F-actin more densely packed with cells, but the cells exhibit a nearly uniform distribution throughout the defects. The similar phenomena are not detected in both blank and PFS groups (Fig. 5A). These results indicate that, the autologous cells seem to only grow at the edge of the defect in the blank and PFS groups, however, the ca-CGMSs facilitate enhanced recruitment and ingrowth of autologous cells into the tissue defect with a uniform distribution and also provide favorable microenvironments for *in situ* cell flourishing expansion (Fig. 5C), thereby offering potential benefits for neo-tissue formation and defect repair.

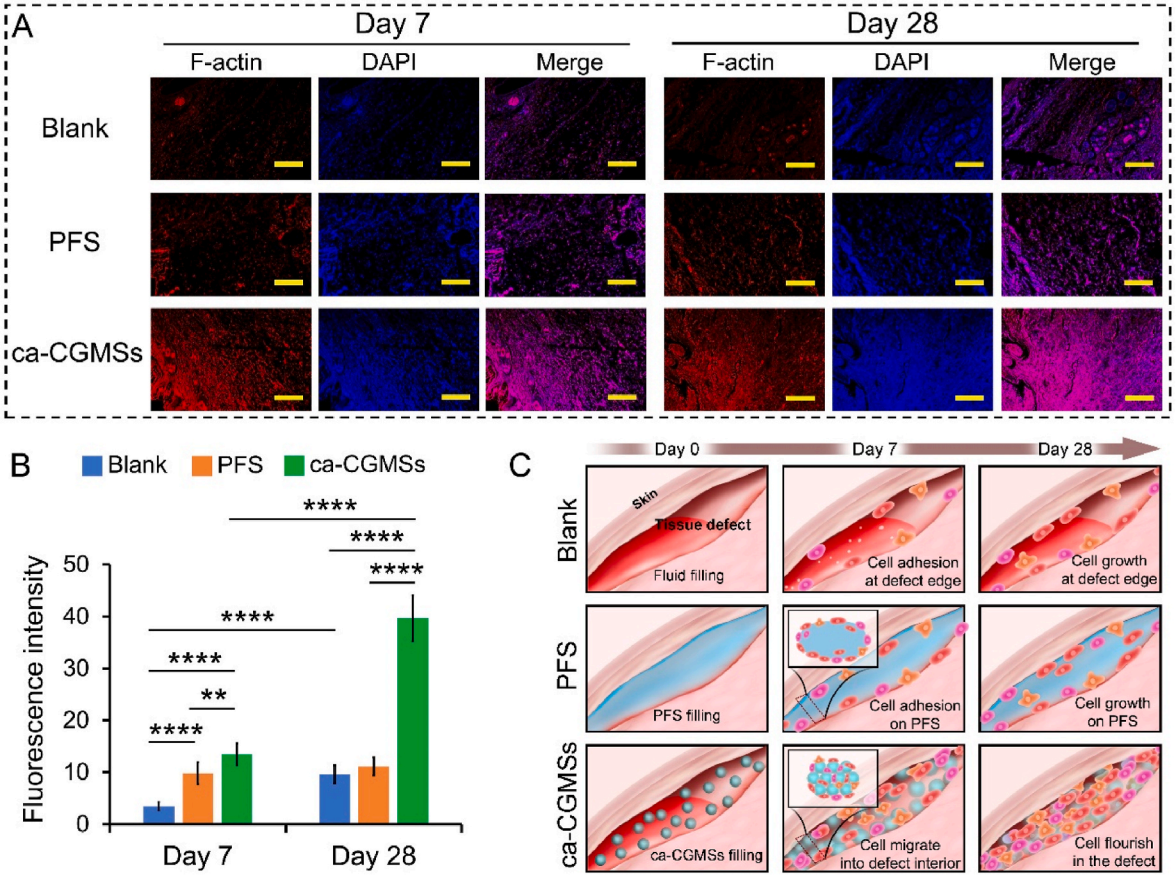

Fig. 5. The ca-CGMSs promote the ingrowth of autologous cells into tissue defects. (A) F-actin staining of the tissue defects treated with PFS or ca-CGMSs, or not treated (Blank); scale bar is 300 μm. (B) Quantification of cell (nucleus) density in the tissue defects; statistical significance is indicated with ** ($p \leq 0.01$), and **** ($p \leq 0.0001$) ($n = 5$). (C) Schematic demonstration of cell recruitments in the three groups, respectively.

3.8. ca-CGMSs promote vascularized neo-tissue formation and wound healing

Subsequently, we performed H&E and Masson's trichome staining to assess tissue repair and wound healing (Fig. 6A). Upon examination of H&E staining images, we have find a significant difference in the repair of tissue defects among the three groups 7 days post-surgery. In the blank group, the extracellular matrix (ECM) is sparsely distributed in the defect, with a significantly lower density than that in the PFS and ca-CGMS groups (Fig. 6B). The central region of the defect in the PFS group exhibits a similarly scattered and disorganized ECM deposition. On the contrary, the ECM in the ca-CGMS group displays higher density and a more ordered arrangement. Similarly, 28 days post-surgery, the ECM in the repair region demonstrates greater density in the ca-CGMS group than in the PFS and blank groups. Furthermore, the density of the ECM deposited in ca-CGMS group obviously increases from Day 7–28. However, this phenomenon has not been clearly detected in PFS group. These observations indicate the superiority of ca-CGMSs as

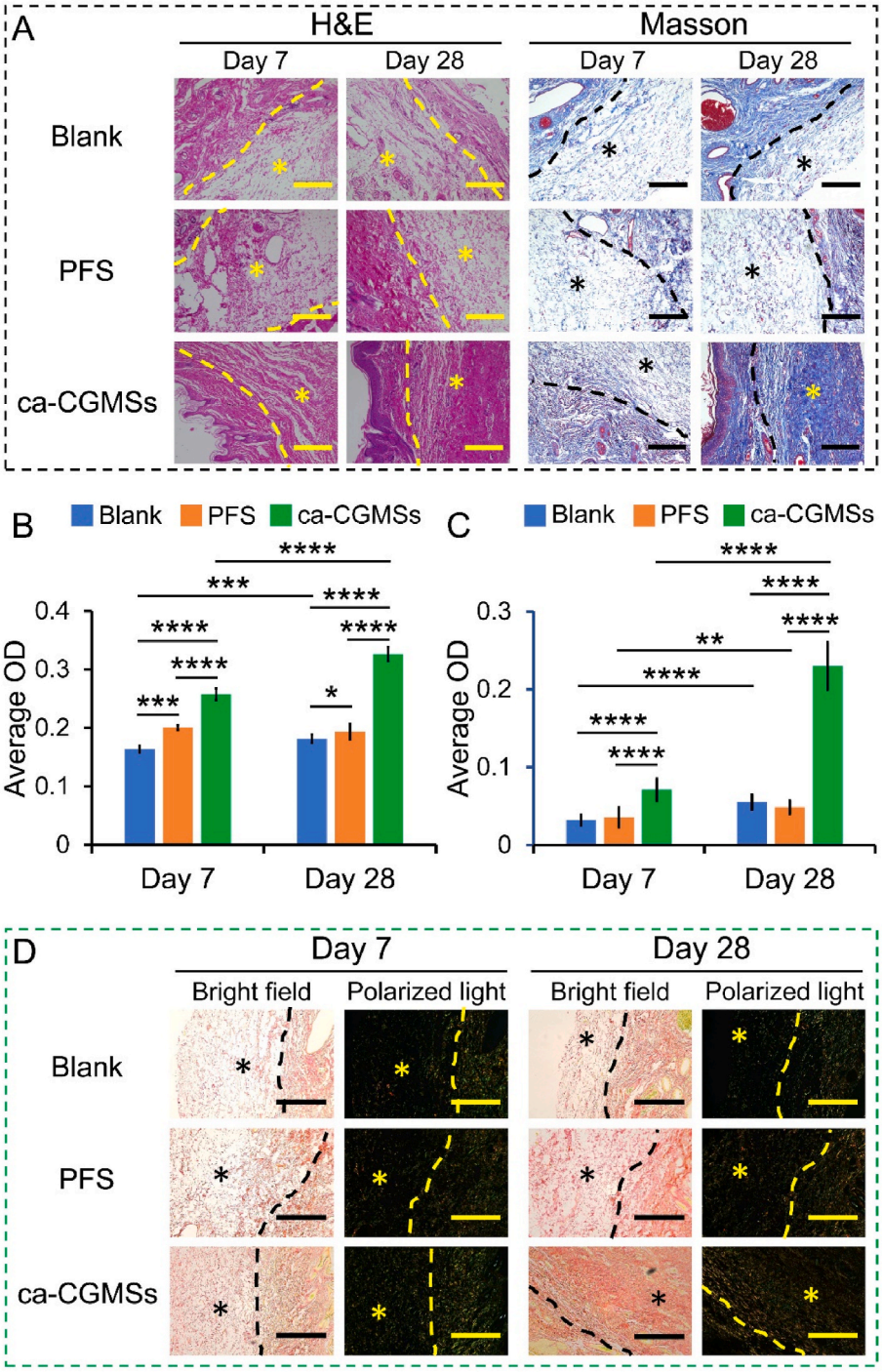

Fig. 6. Promotion of subcutaneous wound healing by ca-CGMSs in the rabbit mastectomy models. (A) Histological staining of formed neo-tissue with hematoxylin and eosin (H&E) and Masson Trichrome in three groups; * indicates the sites of tissue defects; scale bar is 300 μm. Quantification of the deposited extracellular matrix (ECM) after (B) H&E and (C) Masson Trichrome staining, respectively; statistical significance is indicated with * ($p \leq 0.05$), ** ($p \leq 0.01$), *** ($p \leq 0.001$), and **** ($p \leq 0.0001$) ($n = 5$). (D) Sirius red staining of formed neo-tissue; * indicates the sites of tissue defects; scale bar is 200 μm.

restorative implants in providing a more conducive microenvironment for the growth and ECM secretion of the recruited autologous cells. These results further indicate that the gluing of the skin and subcutaneous tissue with PFS can inhibit fluid accumulation by forming physical barriers, however, as illustrated in Fig. 5C, the dense gel structure also restricts cell migration to into its interiors that will hinder the formation of neo-tissue in tissue defect [13]. In other words, the PFS hydrogel can prevent seroma formation to a certain extent, yet it also inhibits cell ingrowth into tissue defect and ECM formation. Upon careful observation, interestingly, the ECM formed in the ca-CGMS group exhibits minimal disparity compared to the surrounding native skin tissue, implying the formation of dense connective neo-tissue. To investigate the fiber types of collagen components in the neo-tissue, we perform Masson's trichome staining (Fig. 6A) [42]. The distribution of ECM is similar to the observations through H&E staining: at each time point, ECM density in the ca-CGMS group is significantly higher than that in the PFS and blank groups (Fig. 6C). Notably, similar to adjacent skin tissue, the neo-tissue displays blue color, indicating the most of

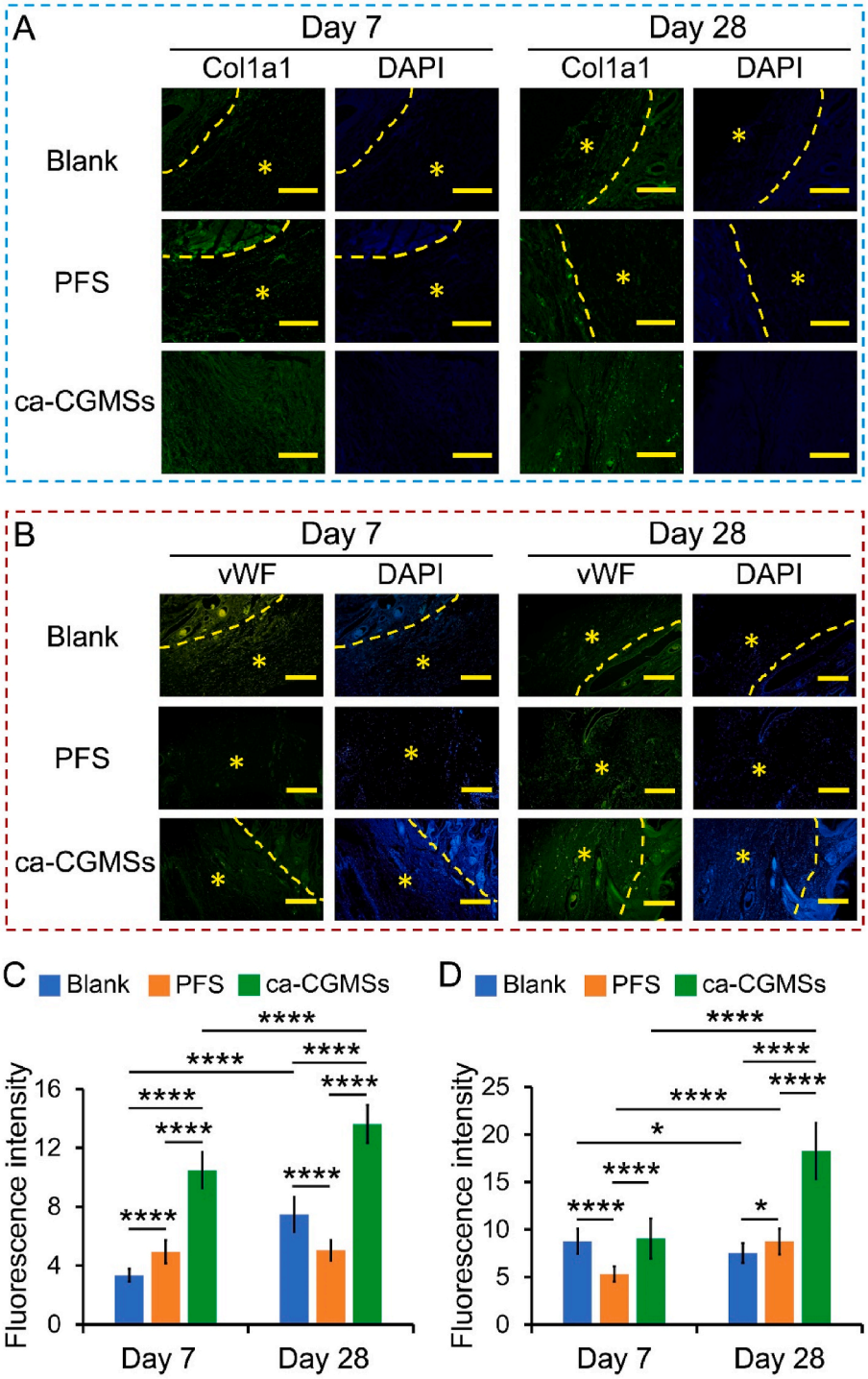

Fig. 7. The ca-CGMSs mediated neo-tissue formation in tissue defects in the rabbit mastectomy models. (A) The immunofluorescent stainings of (A) Col1 (the major ECM protein) and (B) vWF (one crucial angiogenic marker), respectively; * indicates the sites of tissue defects; scale bar is 300 μm. Quantification of the deposited (C) Col1 and (D) vWF, respectively; statistical significance is indicated with * ($p \leq 0.05$), and **** ($p \leq 0.0001$) ($n = 5$).

ECM is collagen fibril [42].

To further distinguish the types of collagen fibrils, we stain the samples with sirius red and followed by examination through a (polarized light) microscopy [43]. As shown in Fig. 6D, under bright-field observation, an increase in collagen fibril deposition is evident over time (from days 7–28). The deposition of collagen fibers is significantly denser in ca-CGMS group than that in the PFS and blank groups, respectively at each time point (Fig. S8, Supplementary material), demonstrating that the ca-CGMSs can provide a superior microenvironment for the secretion of collagen fibril. Under polarized light, collagen fibers appeared predominantly orange-yellow, indicative of primarily Col1 fiber composition in the neo-tissue. At 7 and 28 days post-operation, the blank group exhibits markedly fewer Col1 fibers compared to the PFS and ca-CGMS groups, exhibiting a loose and disordered arrangement. Moreover, Col1 fibers are more densely distributed in the ca-CGMS group compared with the PFS group at both time points. By day 28, in the ca-CGMS group, collagen fibers have nearly fully filled the defect area and exhibited a pattern similar to adjacent tissues.

Subsequently, the formation of vascularized neo-tissue is further studied by immunostaining of the main ECM component of connective tissue (i.e., Col1) and angiogenic markers (i.e., vWF, CD31, VEGF, and HIF-1α) (Figs. 7 and 8) [21,44]. Consistent with the above-mentioned results of histochemical stainings, at Day 7 post-surgery, the blank group exhibits a minimum secretion of Col1 compared to the other two groups (Fig. 7A–C). The ca-CGMS group shows the significantly higher secretion of Col1 than the blank and PFS groups. Similarly, at Day 28, the highest Col1 density is also observed in ca-CGMS group with uniform distribution within the defect site. These results demonstrate that the ca-CGMSs can strikingly induce *in situ* Col1 secretion of the captured autologous cells, which thereby promotes the formation of neo-tissue compared with the blank and PFS.

Adequate vascularization is crucial for the maturation of the regenerated tissues. Consequently, the expression of angiogenic markers has been explored in the three groups. Similar to the observations in Col1 staining, all angiogenic markers are more densely stained in the ca-CGMS group than those in blank and PFS groups (Fig. 7B–D and Fig. 8), and moreover, their expressions are elevated from day 7–28 in ca-CGMS group. These findings show the high capability of ca-CGMSs scaffold in recruiting endogenous angiogenic cell populations (e.g., endothelial cell) and subsequently promoting *in situ* angiogenesis. Interestingly, the expressions of these angiogenic markers in PFS group are even lower than those in blank group at Day 7, which may result from the inhibitory effect of PFS gel body on migration of the angiogenic cells, as illustrated in Fig. 5C. The increased expressions of angiogenic markers (i.e., vWF, CD31, VEGF, and HIF-1α) from Day 7–28 in PFS group should be attributed to the degradation of PFS gel. Above results and findings have demonstrated the superior functions of the ca-CGMSs

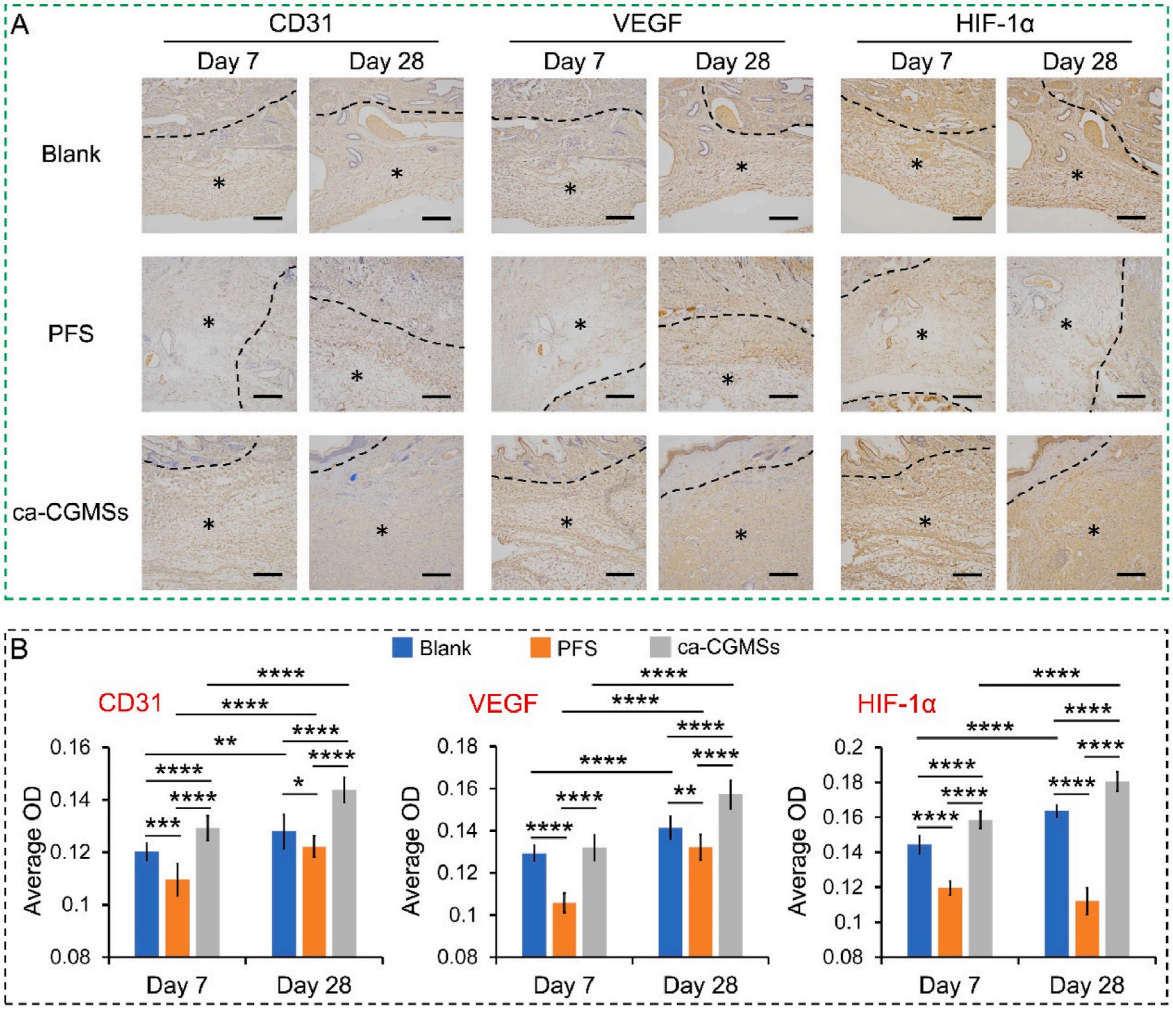

Fig. 8. The ca-CGMSs mediated the enhanced vascularization of the neo-tissue. (A) Immunohistochemistry staining of angiogenic markers, i.e., CD31, VEGF, and Hif-1α, respectively. * indicates the sites of tissue defects; scale bar is 300 μm. (B) Quantification for the deposited CD31, VEGF, and Hif-1α, respectively; statistical significance is indicated with * ($p \leq 0.05$), ** ($p \leq 0.01$), *** ($p \leq 0.001$), and **** ($p \leq 0.0001$) ($n = 5$).

in promoting the healing of subcutaneous wound as well as the formation of vascularized neo-tissue.

Recurrent seroma formation and delayed wound healing post-surgery, will result in improper skin integration with basal muscles or/and flap necrosis, which present major clinical challenges. However, the current methods, namely the use of negative pressure drainage and tissue adhesives, is unable to achieve satisfactory treatment outcomes. To verify our hypothesis that the dried ca-CGMSs will absorb seroma fluid and enhance wound healing by rapidly recruiting autologous cells and promoting tissue regeneration, in this study, we first design and prepare the ca-CGMSs. SEM and optical images show that the ca-CGMSs are manifested as dispersed spheres with a regular shape and a smooth surface (Fig. 2E). They can absorb PBS up to approximately 7-fold of its own weight (Fig. 2F), and exhibit a particle size distribution ranging from 50 to 350 μm in PBS (Fig. 2H). These results indicate the dried ca-CGMSs hold the capacity of absorbing seroma fluid around wound *in vivo* and should be feasible to fill irregular subcutaneous dead spaces.

The efficacy of ca-CGMSs on the promotion of cell proliferation and migration *in vitro* has been studied by comparing with commercial PFS. The results show that PFS merely offers an adhesive interface for cell growth without enabling cell migration into its interior, indicating the significant physical barrier of PFS gel body on cell ingrowth. In contrast, the loosely packed ca-CGMSs can not only provide a substantial substrates (namely microsphere surface) for cell adhesion and proliferation but also facilitate cell migration across the whole ca-CGMSs scaffold due to the interconnected pores among microspheres (Fig. 3C), suggesting the great potential of the ca-CGMSs scaffold in recruiting endogenous cells *in vivo*.

Subsequently, the capability of ca-CGMSs in wet tissue sticking and recruitment of endogenous cells are explored by implanting dried ca-CGMSs into rat mastectomy models. We find the *in situ* swollen ca-CGMSs achieved by absorbing subcutaneous fluid not only aggregate and firmly stick onto the wet tissue (Fig. 4B–Video S1, Supplementary material), but also capture lots of autologous cells that adhere onto the surfaces of ca-CGMSs (Fig. 4D and E). These findings demonstrate the amazing capability of ca-CGMSs in absorbing seroma fluid and promoting cell recruitment *in vivo*.

On account of the preliminary but encouraging discoveries, we next investigate the applicability of dried ca-CGMSs in inhibiting seroma formation as well as promoting subcutaneous tissue healing in rabbit mastectomy models compared with blank and PFS groups. We find the implantation of dried ca-CGMSs significantly inhibit the formation of seroma compared with treating with PFS gluing and no treating (blank) (Fig. 4G). Compared to blank and PFS groups, the strikingly lower fluid accumulation in the ca-CGMS group, especially at day 1 post-surgery, should be attributed to the absorption properties of dried ca-CGMSs. Subsequently, we find the increased cell adhesion, ingrowth, and proliferation in the ca-CGMSs than blank and PFS groups, demonstrating the superiority of ca-CGMSs in recruiting endogenous cells as well as offering conducive environments for enhancing cell proliferation (Fig. 5). Compared with blank and PFS groups, the increased ECM deposition (e.g., Col1) and increased expression of angiogenic markers (e.g., vWF, CD31, VEGF, and HIF-1α) in the ca-CGMS group, further proves the excellent ability of ca-CGMSs to provide a beneficial environment for promoting vascularized neo-tissue formation. Above results demonstrate the multi-functions of ca-CGMSs in absorbing seroma fluid, recruiting endogenous cells, and providing abundant substrates for cell adhesion, proliferation, and ECM secretion as well as vascularized neo-tissue regeneration, ultimately achieving reduced seroma formation and enhanced wound healing.

4. Conclusion

All results and findings of *in vitro* and *in vivo* trials have demonstrated the successful development of the multifunctional ca-CGMSs as well as their availability to inhibit seroma formation and promote wound healing. The ca-CGMSs possessing loose-packed structures, can provide numerous cell-adhesive substrates and interconnected porous structures for cell adhesion, proliferation, and migration to form a whole construct with uniform cell distribution both *in vitro* and *in vivo*, which overcomes the limitations of gel based tissue adhesives (e.g., PFS) on cell migration. The swelling aggregation of the dried ca-CGMSs by absorbing subcutaneous fluid, as well as their capabilities in achieving wet tissue adhesion and cell recruitment have been confirmed in rat mastectomy models. Furthermore, the dried ca-CGMSs not only effectively prevent seroma fluid accumulation but also promote the *in situ* tissue regeneration, enhancing would healing in rabbit mastectomy models. Beyond mastectomy, ca-CGMSs-mediated fluid absorption and tissue repair, mays serve as an efficient methodology to prevent seroma formation and promote wound healing in clinical practices.

CRediT authorship contribution statement

Xinping Wang: Writing – original draft, Software, Investigation, Data curation. **Guoqing Wang:** Writing – original draft, Software, Methodology, Investigation, Data curation. **Jianfei Wang:** Software, Investigation, Data curation. **Junqiang Xue:** Investigation, Formal analysis, Conceptualization. **Gaoli Liu:** Methodology, Investigation, Conceptualization. **Changjiang Fan:** Writing – review & editing, Writing – original draft, Supervision, Funding acquisition, Formal analysis, Conceptualization.

Declaration of competing interest

The authors declare that they have no known competing financial interests or personal relationships that could have appeared to influence the work reported in this paper.

Acknowledgements

The work was financially supported by the National Natural Science Foundation of China (Grant No. 82172108), and Natural Science Foundation of Shandong Province, China (Grant No. ZR2023YQ063, ZR2021MB036).

Appendix A. Supplementary data

Supplementary data to this article can be found online at https://doi.org/10.1016/j.mtbio.2024.101313.

Data availability

Data will be made available on request.

References

[1] F. Bertucci, C.K.Y. Ng, A. Patsouris, N. Droin, S. Piscuoglio, N. Carbuccia, J. C. Soria, A.T. Dien, Y. Adnani, M. Kamal, S. Garnier, G. Meurice, M. Jimenez, S. Dogan, B. Verret, M. Chaffanet, T. Bachelot, M. Campone, C. Lefeuvre, H. Bonnefoi, F. Dalenc, A. Jacquet, M.R. De Filippo, N. Babbar, D. Birnbaum, T. Filleron, C. Le Tourneau, F. Andre, Genomic characterization of metastatic breast cancers, Nature 569 (7757) (2019) 560, https://doi.org/10.1038/s41586-019-1056-z.

[2] L. De Rooij, J.W.A.M. Bosmans, S.M.J. van Kuijk, Y.L.J. Vissers, G.L. Beets, J. van Bastelaar, A systematic review of seroma formation following drain-free mastectomy, Ejso 47 (4) (2021) 757–763, https://doi.org/10.1016/j.ejso.2020.10.010.

[3] L. De Rooij, S.M.J. van Kuijk, E.R.M. van Haaren, A. Janssen, Y.L.J. Vissers, G. L. Beets, J. van Bastelaar, Negative pressure wound therapy does not decrease postoperative wound complications in patients undergoing mastectomy and flap fixation, Sci. Rep. 11 (1) (2021) 9620, https://doi.org/10.1038/s41598-021-89036-3.

[4] N.C. Oleck, C. Gu, B.J. Pyfer, B.T. Phillips, Defining mastectomy skin flap necrosis: a systematic review of the literature and a call for standardization, Plast. Reconstr. Surg. 149 (5) (2022) 858e–866e, https://doi.org/10.1097/prs.0000000000008983.

[5] I. Lese, C. Tsai, M. Matter, T. Wuthrich, H.S. Scheer, A. Taddeo, M. A. Constantinescu, I.K. Herrmann, R. Olariu, Mixed metal oxide nanoparticle formulations for the treatment of seroma, ACS Biomater. Sci. Eng. 7 (6) (2021) 2676–2686, https://doi.org/10.1021/acsbiomaterials.1c00283.

[6] L. Shojaee, S. Sayyadi, R. Amani, A. Nezamtabar Malekshah, Investigating the effect of suture flap fixation on seroma formation in breast cancer patients undergoing mastectomy, Eur. J. Plast. Surg. 46 (6) (2023) 1093–1098, https://doi.org/10.1007/s00238-023-02109-6.

[7] M. Jin, C. Tao, X. Hu, B. Liu, C. Ma, Z. Wu, H. Yao, D.-A. Wang, An instant underwater tissue adhesive composed of catechin-chondroitin sulfate and cholesterol-polyethyleneimine, Adv. Healthcare Mater. 12 (13) (2023) e2202814, https://doi.org/10.1002/adhm.202202814.

[8] K.J. Seong, E.P. Seon, J.S. Lee, L.J. Woo, K.Y. Choi, C.H.O. Yun, C. Byung-Chae, L. Jeeyeon, P.H. Yong, Y.J. Dug, Effect of collagen-enhanced fibrin sealant on seroma formation in a rat mastectomy model, Journal of Wound Management and Research 16 (3) (2020) 137–143, https://doi.org/10.22467/jwmr.2020.01242.

[9] M. Faisal, S. Salem, N. Kamel, H. Abd-Elzaher, A.A. Bakr, H. Fathy, Effect of autologous fibrin glue on seroma reduction after modified radical mastectomy for breast cancer: a randomized controlled trial, Annals of Medicine and Surgery 63 (2021) 102135, https://doi.org/10.1016/j.amsu.2021.01.083.

[10] J.E. Marquez, K. Kapadia, K. Ghosh, B. Silvestri, G. Singh, T.L. Huston, Efficacy of fibrin sealants in preventing seroma formation in reduction mammaplasty: a single surgeon's experience, Ann. Plast. Surg. 85 (2020) S41–S43, https://doi.org/10.1097/sap.0000000000002327.

[11] C. Fan, J. Fu, W. Zhu, D.-A. Wang, A mussel-inspired double-crosslinked tissue adhesive intended for internal medical use, Acta Biomater. 33 (2016) 51–63, https://doi.org/10.1016/j.actbio.2016.02.003.

[12] W. Zhu, J. Yang, J. Iqbal, Y. Peck, C. Fan, D.-A. Wang, A mussel-inspired double-crosslinked tissue adhesive on rat mastectomy model: seroma prevention and in vivo biocompatibility, J. Surg. Res. 215 (2017) 173–182, https://doi.org/10.1016/j.jss.2017.03.020.

[13] C. Fan, D.-A. Wang, Effects of permeability and living space on cell fate and neo-tissue development in hydrogel-based scaffolds: a study with cartilaginous model, Macromol. Biosci. 15 (4) (2015) 535–545, https://doi.org/10.1002/mabi.201400453.

[14] G. An, F. Guo, X. Liu, Z. Wang, Y. Zhu, Y. Fan, C. Xuan, Y. Li, H. Wu, X. Shi, C. Mao, Functional reconstruction of injured corpus cavernosa using 3D-printed hydrogel scaffolds seeded with HIF-1α-expressing stem cells, Nat. Commun. 11 (1) (2020) 2687, https://doi.org/10.1038/s41467-020-16192-x.

[15] H.-s. Ha, S. Baek, K. Lee, S. Cho, M.J. Cho, S. Chung, H. Choi, C.H. Lee, M.S. Kim, S. Y. Kim, D.-H. Kim, S.-W. Kang, H.-J. Sung, Artificial vasa-vasorum serves as an on-site regenerative promoter of cell-free vascular grafting, Adv. Funct. Mater. (2024) 2315310, https://doi.org/10.1002/adfm.202315310.

[16] B.M. Bakadia, A.A.Q. Ahmed, L. Lamboni, Z. Shi, B.M. Mukole, R. Zheng, M. P. Mbang, B. Zhang, M. Gauthier, G. Yang, Engineering homologous platelet-rich plasma, platelet-rich plasma-derived exosomes, and mesenchymal stem cell-derived exosomes-based dual-crosslinked hydrogels as bioactive diabetic wound dressings, Bioact. Mater. 28 (2023) 74–94, https://doi.org/10.1016/j.bioactmat.2023.05.002.

[17] B. Salahuddin, S. Wang, D. Sangian, S. Aziz, Q. Gu, Hybrid gelatin hydrogels in nanomedicine applications, ACS Appl. Bio Mater. 4 (4) (2021) 2886–2906, https://doi.org/10.1021/acsabm.0c01630.

[18] Z. Dong, X. Meng, W. Yang, J. Zhang, P. Sun, H. Zhang, X. Fang, D.-A. Wang, C. Fan, Progress of gelatin-based microspheres (GMSs) as delivery vehicles of drug and cell, Mater. Sci. Eng., C 122 (2021) 111949, https://doi.org/10.1016/j.msec.2021.111949.

[19] C. Fan, S.-H. Zhan, Z.-X. Dong, W. Yang, W.-S. Deng, X. Liu, D.-A. Wang, P. Sun, Cross-linked gelatin microsphere-based scaffolds as a delivery vehicle of MC3T3-E1 cells: in vitro and in vivo evaluation, Mater. Sci. Eng., C 108 (2020) 110399, https://doi.org/10.1016/j.msec.2019.110399.

[20] Z. Dong, C. Fan, W. Deng, P. Sun, Porous gelatin microsphere-based scaffolds containing MC3T3-E1 cells and calcitriol for the repair of skull defect, Biomater. Adv. 138 (2022) 212964, https://doi.org/10.1016/j.bioadv.2022.212964.

[21] P. Wang, X. Meng, R. Wang, W. Yang, L. Yang, J. Wang, D.-A. Wang, C. Fan, Biomaterial scaffolds made of chemically cross-linked gelatin microsphere aggregates (C-GMSs) promote vascularized bone regeneration, Adv. Healthcare Mater. 11 (13) (2022) e2102818, https://doi.org/10.1002/adhm.202102818.

[22] H. Ke, H. Yang, Y. Zhao, T. Li, D. Xin, C. Gai, Z. Jiang, Z. Wang, 3D gelatin microsphere scaffolds promote functional recovery after spinal cord hemisection in rats, Adv. Sci. 10 (3) (2023) e2204528, https://doi.org/10.1002/advs.202204528.

[23] Z. Wang, X. Zhang, L. Xue, G. Wang, X. Li, J. Chen, R. Xu, T. Xu, A controllable gelatin-based microcarriers fabrication system for the whole procedures of MSCs amplification and tissue engineering, Regenerative Biomaterials 10 (2023) rbad068, https://doi.org/10.1093/rb/rbad068.

[24] J. Zhu, Q. Luo, G. Yang, L. Xiao, Biofabrication of tissue-engineered cartilage constructs through faraday wave bioassembly of cell-laden gelatin microcarriers, Adv. Healthcare Mater. (2024) e2304541, https://doi.org/10.1002/adhm.202304541.

[25] X. Li, X. Li, J. Yang, J. Lin, Y. Zhu, X. Xu, W. Cui, Living and injectable porous hydrogel microsphere with paracrine activity for cartilage regeneration, Small 19 (17) (2023) e2207211, https://doi.org/10.1002/smll.202207211.

[26] K. Feng, Y. Yu, Z. Chen, F. Wang, K. Zhang, H. Chen, J. Xu, Q. Kang, Injectable hypoxia-preconditioned cartilage progenitor cells-laden GelMA microspheres system for enhanced osteoarthritis treatment, Materials Today Bio 20 (2023) 100637, https://doi.org/10.1016/j.mtbio.2023.100637.

[27] J. Li, Y. Wu, Q. Yuan, L. Li, W. Qin, J. Jia, K. Chen, D. Wu, X. Yuan, Gelatin microspheres based on H8-loaded macrophage membrane vesicles to promote wound healing in diabetic mice, ACS Biomater. Sci. Eng. 10 (4) (2024) 2251–2269, https://doi.org/10.1021/acsbiomaterials.3c01742.

[28] H. Liu, X. Tian, C. Jin, Y. Li, X. Zhu, M. Pei, T. Liu, H. Yang, Y. Xu, F. He, Delivering cells via ECM mimetic hydrogel microspheres for promoting the reconstruction of rat lumbar nucleus pulposus, Chem. Eng. J. 486 (2024) 150212, https://doi.org/10.1016/j.cej.2024.150212.

[29] M. Dong, X. Yang, J. Lu, L. Siow, H. He, A. Liu, P. Wu, Y. He, M. Sun, M. Yu, H. Wang, Injectable rBMSCs-laden hydrogel microspheres loaded with naringin for osteomyelitis treatment, Biofabrication 15 (4) (2023), https://doi.org/10.1088/1758-5090/aceaaf.

[30] G. Wang, X. Meng, P. Wang, X. Wang, G. Liu, D.-A. Wang, C. Fan, A catechol bioadhesive for rapid hemostasis and healing of traumatic internal organs and major arteries, Biomaterials 291 (2022) 121908, https://doi.org/10.1016/j.biomaterials.2022.121908.

[31] W. Zhang, R. Wang, Z. Sun, X. Zhu, Q. Zhao, T. Zhang, A. Cholewinski, F. Yang, B. Zhao, R. Pinnaratip, P.K. Forooshani, B.P. Lee, Catechol-functionalized hydrogels: biomimetic design, adhesion mechanism, and biomedical applications, Chem. Soc. Rev. 49 (2) (2020) 433–464, https://doi.org/10.1039/c9cs00285e.

[32] Z. Hu, W. Wu, M. Yu, Z. Wang, Z. Yang, X. Xing, X. Chen, L. Niu, F. Yu, Y. Xiao, J. Chen, Mussel-inspired polymer with catechol and cationic Lys functionalities for dentin wet bonding, Materials Today Bio 18 (2023) 100506, https://doi.org/10.1016/j.mtbio.2022.100506.

[33] S. Wang, J. Liu, L. Wang, H. Cai, Q. Wang, W. Wang, J. Shao, X. Dong, Underwater adhesion and anti-swelling hydrogels, Advanced Materials Technologies 8 (6) (2023), https://doi.org/10.1002/admt.202201477.

[34] K. Wu, M. Fu, Y. Zhao, E. Gerhard, Y. Li, J. Yang, J. Guo, Anti-oxidant anti-inflammatory and antibacterial tannin-crosslinked citrate-based mussel-inspired bioadhesives facilitate scarless wound healing, Bioact. Mater. 20 (2023) 93–110, https://doi.org/10.1016/j.bioactmat.2022.05.017.

[35] C. Sun, X. Zeng, S. Zheng, Y. Wang, Z. Li, H. Zhang, L. Nie, Y. Zhang, Y. Zhao, X. Yang, Bio-adhesive catechol-modified chitosan wound healing hydrogel dressings through glow discharge plasma technique, Chem. Eng. J. 427 (2022) 130843, https://doi.org/10.1016/j.cej.2021.130843.

[36] L. Wang, Z. Zhao, J. Dong, D. Li, W. Dong, H. Li, Y. Zhou, Q. Liu, B. Deng, Mussel-inspired multifunctional hydrogels with adhesive, self-Healing, antioxidative, and antibacterial activity for wound healing, ACS Appl. Mater. Interfaces 15 (13) (2023) 16515–16525, https://doi.org/10.1021/acsami.3c01065.

[37] M.S. Choi, H.K. Kim, W.S. Kim, T.H. Bae, M.K. Kim, A comparison of triamcinolone acetonide and fibrin glue for seroma prevention in a rat mastectomy model, Ann. Plast. Surg. 69 (2) (2012) 209–212, https://doi.org/10.1097/SAP.0b013e318226b516.

[38] S. Hong, K. Yang, B. Kang, C. Lee, I.T. Song, E. Byun, K.I. Park, S.-W. Cho, H. Lee, Hyaluronic acid catechol: a biopolymer exhibiting a pH-dependent adhesive or cohesive property for human neural stem cell engineering, Adv. Funct. Mater. 23 (14) (2013) 1774–1780, https://doi.org/10.1002/adfm.201202365.

[39] Y. Li, J. Li, S. Jiang, C. Zhong, C. Zhao, Y. Jiao, J. Shen, H. Chen, M. Ye, J. Zhou, X. Yang, Z. Gou, S. Xu, M. Shen, The design of strut/TPMS-based pore geometries in bioceramic scaffolds guiding osteogenesis and angiogenesis in bone regeneration, Materials Today Bio 20 (2023) 100667, https://doi.org/10.1016/j.mtbio.2023.100667.

[40] S. Guo, C. He, Bioprinted scaffold remodels the neuromodulatory microenvironment for enhancing bone regeneration, Adv. Funct. Mater. 33 (40) (2023) 2304172, https://doi.org/10.1002/adfm.202304172.

[41] Q. Meng, B. Ding, P.a. Ma, J. Lin, Interrelation between programmed cell death and immunogenic cell death: take antitumor nanodrug as an example, Small Methods 7 (5) (2023) e2201406, https://doi.org/10.1002/smtd.202201406.

[42] L. Becker, C.-E. Lu, I.A. Montes-Mojarro, S.L. Layland, S. Khalil, A. Nsair, G. P. Duffy, F. Fend, J. Marzi, K. Schenke-Layland, Raman microspectroscopy identifies fibrotic tissues in collagen-related disorders via deconvoluted collagen type I spectra, Acta Biomater. 162 (2023) 278–291, https://doi.org/10.1016/j.actbio.2023.03.016.

[43] H. Gao, L. Wang, Z. Lin, H. Jin, Y. Lyu, Y. Kang, T. Zhu, J. Zhao, J. Jiang, Bi-lineage inducible and immunoregulatory electrospun fibers scaffolds for synchronous regeneration of tendon-to-bone interface, Materials Today Bio 22 (2023) 100749, https://doi.org/10.1016/j.mtbio.2023.100749.

[44] Y. Yu, Y. Leng, X. Song, J. Mu, L. Ma, L. Yin, Y. Zheng, Y. Lu, Y. Li, X. Qiu, H. Zhu, J. Li, D. Wang, Extracellular matrix stiffness regulates microvascular stability by controlling endothelial paracrine signaling to determine pericyte fate, Arterioscler. Thromb. Vasc. Biol. 43 (10) (2023) 1887–1899, https://doi.org/10.1161/atvbaha.123.319119.